Supplementary Materials for

Phosphorus-tungsten dual-doping boosts acidic overall seawater splitting performance over RuO_x nanocrystals

Junyang Ding[a,b]†, Zimo Peng[b]†, Zhiwei Wang[c], Chunhui Zeng[a],Yanhong Feng[c], Miaosen Yang[a]*, Guagnzhi Hu[d], Jun Luo[e], and Xijun Liu[c]**

[a] *School of Chemical Engineering, Northeast Electric Power University, Jilin 132012, Jilin, China*

[b] *Institute for New Energy Materials & Low-Carbon Technologies, School of Materials Science and Engineering, Tianjin University of Technology, Tianjin 300384, China*

[c] *State Key Laboratory of Featured Metal Materials and Life-cycle Safety for Composite Structures, Guangxi Key Laboratory of Processing for Non-ferrous Metals and Featured Materials, MOE Key Laboratory of New Processing Technology for Nonferrous Metals and Materials, School of Resources, Environment and Materials, Guangxi University, Nanning, 530004 Guangxi, China*

[d] *Institute for Ecological Research and Pollution Control of Plateau Lakes School of Ecology and Environmental Science, Yunnan University, Kunming 650504, China*

[e] *ShenSi Lab, Shenzhen Institute for Advanced Study, University of Electronic Science and Technology of China, Longhua District, Shenzhen 518110, China*

Corresponding authors: zengchunhuijia@163.com; ymiaosen@163.com; xjliu@gxu.edu.cn

† These authors contributed equally to this work.

Experimental Section

Structural Characterizations

Powder X-ray diffraction (PXRD, 2θ = 10-80°) measurements were undertaken on a Rigaku SmartLab 9KW diffractometer (Cu K_α, λ = 1.5418 Å). Scanning electron microscopy (SEM, FEI Verios 460 L), transmission electron microscope (TEM, FEI Talos F200 X), and the equipped X-ray electron dispersive spectroscopy (EDS) were conducted to analyze the morphology and composition of the samples. X-ray photoelectron spectroscopy (XPS), using Al K_α radiation, was acquired on a Thermo ESCALAB250Xi, which was then calibrated against the benchmark C 1s (284.8 eV) peak location.

Electrochemical Measurements

Using a standard three-electrode setup at the CHI760E workstation (Chenhua, Shanghai), acidic seawater containing 0.5 M H_2SO_4 or individual 0.5 M H_2SO_4 aqueous solution, and ambient temperature, the two half-reactions of water splitting (i.e., HER and OER) were investigated. The natural seawater is taken from the Yellow Sea of China. The main ions in the real seawater are Cl^- (19300 ppm), K^+ (300 ppm), Na^+ (10800 ppm), Ca^{2+} (400 ppm), Br^- (70 ppm), and Mg^{2+} (1300 ppm). In this system, the Hg/Hg_2SO_4 electrodes (within saturated K_2SO_4) are employed as reference electrodes, while graphite rods (6.0 mm in diameter) serve as counter electrodes. For working electrodes, as-prepared powder electrocatalysts loaded on carbon paper (CP, 1.0 ×2.0 cm^2, Hesen, HCP-020) were employed and their exposed geometrical areas were all fixed at 1.0 cm^2. The preparation procedure was as follows: with the aid of sonication for 30 min, 3 mg of PW-OA-RuO_x@C, 3 mg of carbon black, and 500 μL of Nafion/ethanol solution with a volume ratio of 1/4 were well dispersed together to prepare sample ink, and then coating 200 μL ink on CP and drying it in an oven at 60 ℃. Instead, a pair of PW-OA-RuO_x@C||PW-OA-RuO_x@C electrodes that are identical were used to assess their total water splitting characteristics. All potentials applied were converted to the reversible hydrogen electrode (E_{RHE}) using the formula ($E_{RHE} = E_{Hg/Hg2SO4} + 0.652\ V + 0.059$

× pH) and RHE calibration (Figure S1). The 90% iR-corrected linear sweep voltammetry (LSV) curves with a scan rate of 5 mV s^{-1} were recorded. Within the frequency range from 0.1 to 100000 Hz and an amplitude of 5 mV, the electrochemical impedance spectroscopy (EIS) was carried out. Cyclic voltammetry (CV) curves are measured at various scan rates of 20 ~ 100 mV s^{-1} for calculating the double layer capacitances (C_{dl}) values. The chronopotentiometry tests are configured at a constant current density of 10 mA cm^{-2}.

DFT details

The PW-OA-RuO_x and RuO_2 models were constructed under the density functional theory (DFT) in the VASP. The lattice structure was set to periodic 4 × 2 unit cells, i.e., each structure has three layers of metal atoms including the fixed one layer bottom atom as well as other relaxed two layer atoms for adsorbing objects. According to the characterization analysis results, the model of (110) surface of RuO_2 with incorporated W and P atoms was considered as PW-OA-RuO_x@C. To analyze the Perdew-Burke-Emzerhof (PBE) exchange effect and related influence under the condition of generalized gradient approximation, the vacuum space was set to 15 Å. And, the Brillouin zone was sampled with 1 × 1 × 1. Nuclear processes and atomic charges were analyzed by the effective core potential (ECP) and Hirshfeld method, respectively.

The free energy of atomic structure is determined as follows:

$$\triangle G = \triangle E + \triangle ZPVE + \int C_P dT - T \triangle S,$$

where △E is the change of adsorption energy, △ZPVE is the difference of zero-point energy, and △S is the difference of entropy, C_p is the heat capacity, and T is the system temperature.

Figures and Tables

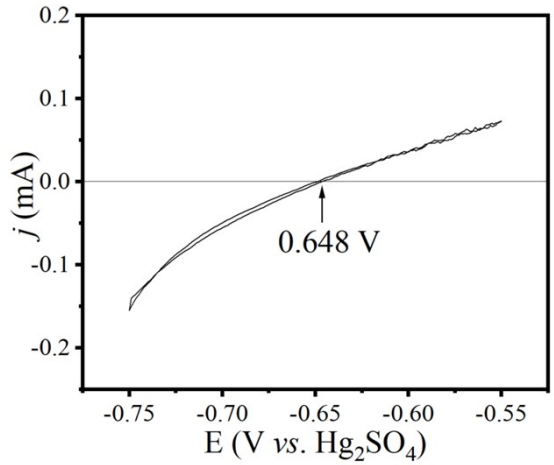

Figure S1. The calibration CVs graph of Hg_2SO_4 electrode vs RHE.

In this work, the high purity hydrogen saturated acidic seawater (0.5 M H_2SO_4 + natural seawater) as the electrolyte, the Hg_2SO_4 electrode as the reference electrode, two Pt sheets (1.0 × 1.0 cm^2) as the working electrode and counter electrode, respectively. As shown in Figure S1, the CVs test with a scan rate of 1 mV s^{-1} is performed and the average of the two potentials at current crossed zero is the correction potential of hydrogen electrode reactions. So in alkaline seawater, $E_{RHE} = E_{Hg/Hg2SO4} + 0.648$ V.

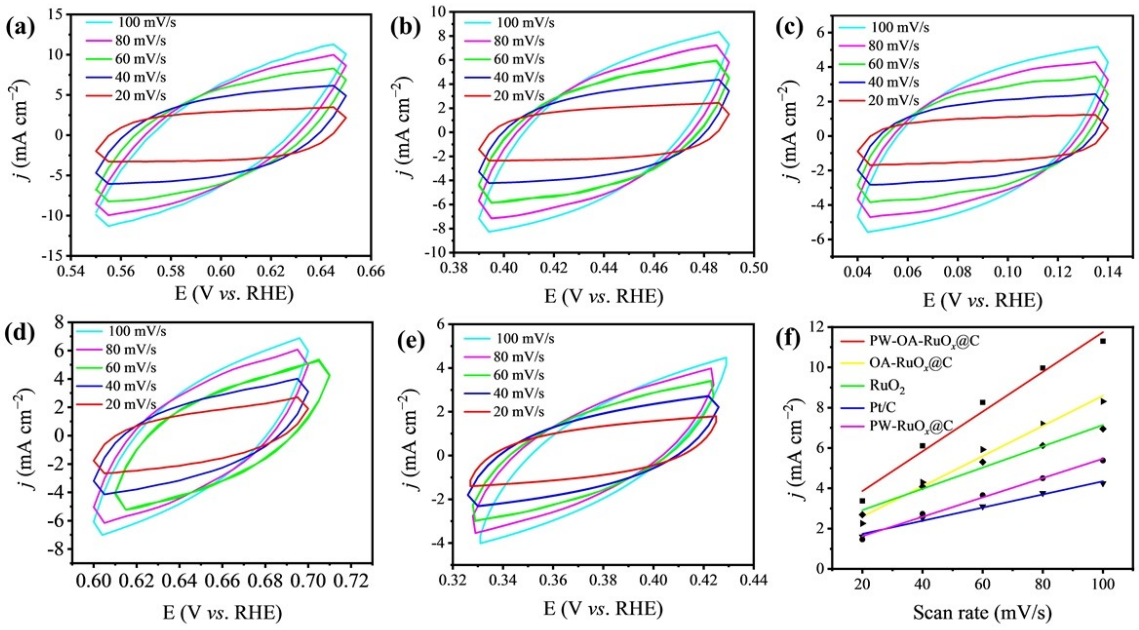

Figure S2. Typical CV curves of (a) PW-OA-RuO_x@C, (b) OA-RuO_x@C, (c) PW-RuO_x@C, (d) RuO_2, (e) Pt/C with different scan rates; (f) C_{dl} of various catalysts.

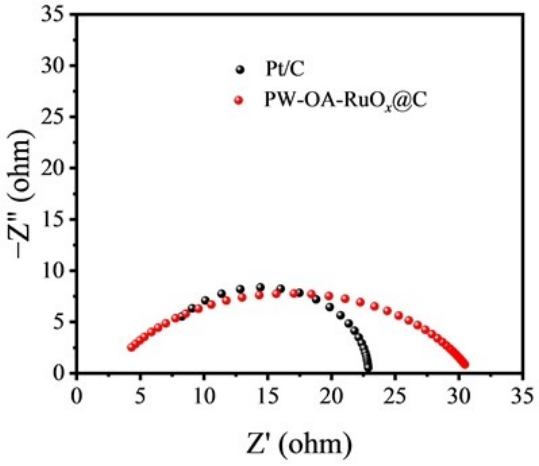

Figure S3. EIS of PW-OA-RuO_x@C and Pt/C.

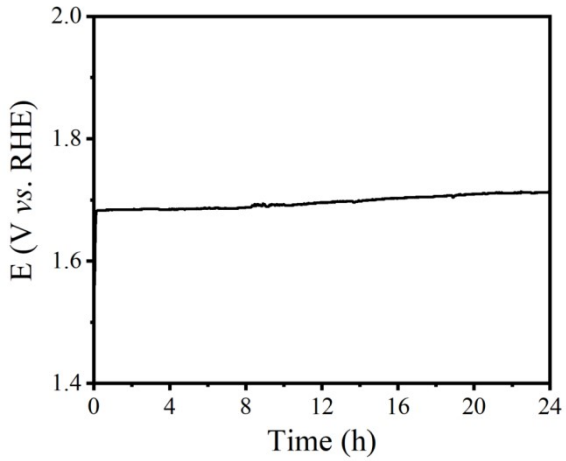

Figure S4. Long-term durability test of the PtC||RuO_2 at the constant current density of 10 mA cm^{-2} for the overall water splitting in acidic seawater.

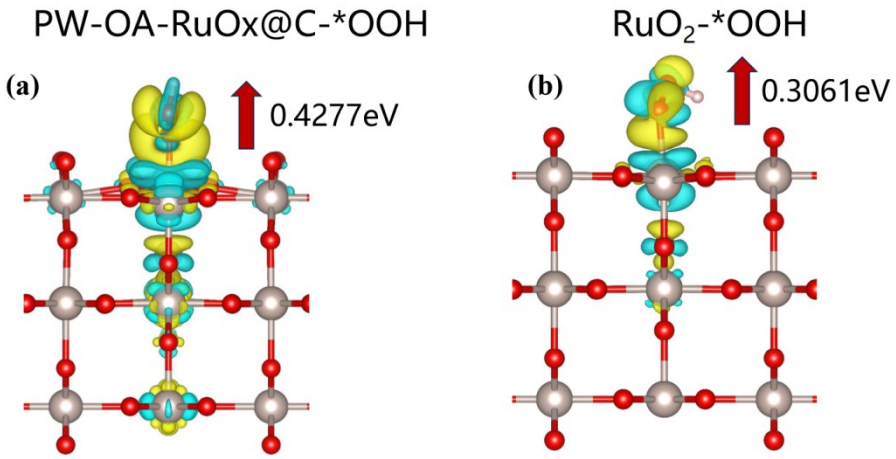

Figure S5. Charge density difference of (a) *OOH on PW-OA-RuO_x@C (110) and (b) *OOH on RuO_2 (110). Note that yellow and cyan shadows represent charge accumulation and depletion in the space, respectively.

Table S1 Comparisons of the HER activity for the PW-OA-RuO_x@C and some recently reported catalysts.

Catalyst	Electrolyte	Overpotential at 10 mA cm^{-2} (mV)	Ref.
PW-OA-RuO_x@C	Acidic seawater	45	This work
	0.5 M H_2SO_4	39	
FeCoCrMoCBY	0.5 M H_2SO_4	62	J. Mater. Sci. Technol. 2024, 170, 212-220.
WC-CFP	0.5 M H_2SO_4	152	J. Energy Chem. 2021, 62, 610-616.
RuIrTe NTs	0.5 M H_2SO_4	29	J. Mater. Chem. A. 2022, 10, 2021-2026.
0.2rGO-MoS_2	0.5 M H_2SO_4	146	Chem. Eng. J. 2021, 418, 129343.
	1.0 M KOH	314	
V-CoP_2/CC	0.5 M H_2SO_4	50	Angew. Chem. Int. Ed. 2022, 61, e202116233.
1T-MoS_2	0.5 M H_2SO_4	136	Chem. Eng. J. 2021, 422, 130100.
$SrHf_{1-x}RuxO_{3-\delta}$	0.5 M H_2SO_4	48	Adv. Funct. Mater. 2023, 33, 2213523.
FeP/Ni_2P/CP	0.5 M H_2SO_4	51	J. Mater. Chem. A. 2022,10, 15569-15579.
	1.0 M KOH	46	

Table S2 Comparisons of the OER activity for the PW-OA-RuO_x@C and some recently reported catalysts.

Catalyst	Electrolyte	Overpotential at 10 mA cm^{-2} (mV)	Ref.
PW-OA-RuO_x@C	Acidic seawater	158	This work
	0.5 M H_2SO_4	241	
IrCoNi PHNCs	0.1 M $HClO_4$	303	Adv. Mater. 2017, 29, 1703798
P-$IrCu_{1.4}$ NCs	0.05 M H_2SO_4	311	Chem. Mater. 2018, 30, 8571.
$RuPbO_x$	0.5 M H_2SO_4	191	Nano Energy. 2022, 104, 107960
3R-IrO_2	0.1 M $HClO_4$	188	Joule, 2021, 5, 3221-3234.
$Bi_xEr_{2-x}Ru_2O_7$	0.1 M $HClO_4$	180	Nat. Commun. 2022, 13, 4106.
Ag_1/IrO_x SAC	0.5 M H_2SO_4	224	ACS Energy Lett. 2021, 6, 4, 1588-1595.
RuO_2/BNNS	0.5 M H_2SO_4	180	Angew. Chem. Int. Ed. 2024, 63, e202402018.
Ru@Ir-O	0.5 M H_2SO_4	238	Small 2022, 18, 2108031

Table S3 Comparisons of the overall water splitting activity for the PW-OA-RuO_x@C and some recently reported catalysts.

Catalyst	Electrolyte	Voltage at 10 mA cm^{-2} (V)	Ref.
PW-OA-RuO_x@C	Acidic seawater	1.47	This work
	0.5 M H_2SO_4	1.49	
Co-SAC/RuO_2	0.5 M H_2SO_4	1.511	J. Mater. Chem. A, 2022, 10, 2021-2026.
np-$Pd_{50}Ir_{50}$	0.5 M H_2SO_4	1.52	J. Mater. Chem. A, 2023,11, 11526-11533
RuO_2-WC NPs	0.5 M H_2SO_4	1.66	Angew. Chem. Int. Ed. 2022, 61, e202202519.
5%Pt-Ru ONAs/C	0.5 M H_2SO_4	1.486	Chin. J. Catal. 2022, 43(6), 1493-1501.
	0.05 M H_2SO_4	1.497	
V-CoP_2/CC	0.5 M H_2SO_4	1.47	Angew. Chem. Int. Ed. 2022, 61, e202116233.
IrNi NCs	0.5 M H_2SO_4	1.58	Adv. Funct. Mater. 2017, 27, 1700886.
RuIr-NC	0.05 M H_2SO_4	1.485	Nat. Commun. 2021, 12, 1145.
Pt-RuO_2@KB	0.1 M $HClO_4$	1.54	J. Mater. Chem. A, 2022,10, 13241-13246.

The assembled PW-OA-RuO_x@C||PW-OA-RuO_x@C acidic water/seawater electrolyzer can be stabilized for 50 h at 10 mA cm^{-2} current densities, and it was discovered that this PW-OA-RuO_x@C electrocatalysts were on par with or even superior to those of these reported catalysts in recent years in Table S3. For the HER/OER half-responses, we also summarize recently reported state-of-the-art materials (Tables S1, S2). For HER, PW-OA-RuO_x@C is comparable to the reported noble metal catalysts and far superior to the non-precious metal catalysts; while for OER, the electrocatalysts are basically focused on Ru-based or Ir-based materials, and PW-OA-RuO_x@C is as superior as these catalysts, which suggests that the high efficiency bifunctional electrocatalytic materials for acid water decomposition still have broad development prospects.